International Journal of
Plasma Environmental Science and Technology

Regular Paper DOI: 10.34343/ijpest.2021.15.e02014

Insight into the improvement of the SO_2 resistance in low-temperature ozone assisted SCR over CeO_2-WO_3 catalyst

Zhengyan Liu[1, 3], Meiyi Liu[1, 3], Nan Jiang[2], Bangfa Peng[2], Jie Li[1, 2, 3, *], Yan Wu[2]

[1] Key Laboratory of Industrial Ecology and Environmental Engineering, Dalian University of Technology, Dalian, China
[2] School of Electrical Engineering, Dalian University of Technology, Dalian, China
[3] School of Environmental Science & Technology, Dalian University of Technology, Dalian, China

* Corresponding author: lijie@dlut.edu.cn (Jie Li)

Received: 9 May 2021
Revised: 20 July 2021
Accepted: 12 August 2021
Published online: 18 August 2021

Abstract

In this work, the SO_2 resistance characteristics of CeO_2-WO_3 catalysts in ozone assisted selective catalytic reduction (O_3-SCR) and SCR systems were comparatively studied. Firstly, a series of CeO_2-WO_3 catalysts with different Ce/W ratios were prepared by the co-precipitation method and evaluated for the selective catalytic reduction of NO_x by ammonia over a wide temperature range. These catalysts were characterized by XRD, BET, XPS and H_2-TPR analysis. The experimental results demonstrated that Ce3W1 catalyst exhibited the best activity toward NH_3-SCR reaction over a broad temperature range of 100−450 °C at the gas hourly space velocity (GHSV) of 25,000 h^{-1}. The O_3-SCR results proved that its NO_x removal performance was significantly higher than that of SCR in the low temperature range (< 200 °C). A comparison of SO_2 resistance performance in O_3-SCR and traditional SCR was conducted. Results showed that the NO_x conversion of O_3-SCR was better than that of SCR under the presence of SO_2 for 5 h at 150 °C. It is worth noting that the results obtained through FTIR, XPS and TG characterization indicated that the sulfate content on the surface of SO_2 poisoned catalyst in O_3-SCR system was remarkably lower. Therefore, O_3-SCR could greatly improve the NO_x conversion at low temperatures and SO_2 durability, thereby achieving the purpose of extending the service life of the catalyst.

Keywords: SCR, O_3, CeO_2-WO_3, SO_2 resistance.

1. Introduction

As one of the main air pollutants, nitrogen oxides (NO_x) emitted from stationary sources such as thermal power plants and cement plants have caused serious environmental pollution and human health problems [1]. In recent years, stricter regulations, and policies to limit nitrogen oxide emissions have been required, and it is urgent to develop and promote efficient and stable NO_x emission control technologies [2]. Ammonia selective catalytic reduction technology (SCR) has been considered as the most dominant technology for controlling NO_x emissions [3]. The major reaction is

$$4NO + 4NH_3 + O_2 \rightarrow 4N_2 + 6H_2O \quad \text{（standard SCR）} \qquad (1)$$

Besides, a fast SCR reaction can occur when NO/NO_2 is 1, which has a faster reaction rate than the standard SCR [4]. The fast SCR response is shown in Eq. 2 [5].

$$NO + NO_2 + 2NH_3 \rightarrow 2N_2 + 3H_2O \quad \text{（fast SCR）} \qquad (2)$$

The partial oxidation of NO to NO_2 by the oxidation method to achieve a rapid SCR reaction can improve the efficiency of flue gas denitration [6]. To approach this purpose, O_3 oxidation with the advantages of quick response, high selectivity and no secondary pollution is usually considered as an efficient method [7]. Currently, one of the most widely used technologies to generate O_3 is the dielectric barrier discharge method which is also utilized in this work with the benefits of wide gas source (dry air, oxygen, or oxygen-containing gas), large output of O_3 and low cost [8−9].

However, in the practical situation, industrial flue gas or tail gas usually contains high concentration of sulfur dioxide which can have side reactions with the catalyst and result in a large amount of ammonium sulfate and ammonium bisulfate [10−11]. These by-products subsequently result in the problem of catalyst blockage and equipment corrosion, which directly affect the stable emission of nitrogen oxides to meet the standard and the long-term operation of the device [12−13]. Mechanism and method to inhibit the sulfur poisoning of the catalysts need to be paid attention in the field of denitration technology. Therefore, the effect of the O_3 assisted SCR compared with the standard SCR on the sulfur resistance should be carried out and give a further understanding.

At present, researches on fixed-source SCR catalysts are mainly focused on transition metal oxides. The doping of transition metal can protect the active component and enhance the catalytic activity [14]. Due to the different physical and chemical properties of various metal elements, there will be different effects on the surface crystal structure, microscopic specific surface area and active site of the denitration catalyst. Especially the active acid site on the surface of the catalyst is closely related to the type and surface density of the metal oxides compound [15]. It is important to find the appropriate metal doping to improve the performance of the catalyst. Commonly used low-temperature catalysts are mainly manganese-based (MnO_x) catalysts [16−17], vanadium-based (VO_x) catalysts [18] and some other metals such as copper-based (CuO) [19], iron-based (FeO_x) [20]. Among these, studies have found that Ce^{3+}/Ce^{4+} redox of cerium has a reversible redox reaction under milder conditions, and has good oxygen storage and release capabilities [21]. Guo *et al*. [22] investigated CeO_2-CuO catalyst prepared by citric acid method, results showed that the abundant oxygen storage capacity of CeO_2 and the emergence of Ce^{3+} may be the main reason why CeO_2-CuO had good SCR performance at low temperatures. Wang *et al*. [23] found that under the optimal condition, the NO conversion of Ce-Co composite catalyst at 230 °C was as high as 93%. On the other hand, researches have reported that as a stabilizer and accelerator, W can significantly increase the specific surface area of the catalyst, and the highly dispersed W element is conducive to the improvement of the catalytic effect of the catalyst [24]. Kobayashi *et al*. [25] found that the WO_3-TiO_2 catalyst prepared by coprecipitation exhibited a higher SCR activity and thermal stability at high temperatures. Zhang *et al*. [26] reported that WO_3 could improve the reducibility and enhanced the amount and strength of the surface Brönsted acid sites. Therefore, in this experiment, a synergism between Ce and W oxide surface species is performed to broaden the reaction temperature window of the catalyst and improve the denitration effect of the catalyst at low temperature.

In this work, we prepared a series of CeO_2-WO_3 catalysts with different Ce/W to investigate their activity in the low temperature SCR in the temperature range of 200−450 °C. The effects of O_3-SCR on NO_x conversion and sulfur resistance of CeO_2-WO_3 catalyst were also investigated. Catalysts were characterized by XRD, XPS, FTIR and TG to explore the deactivation principle of the catalyst.

2. Experimental system

2.1 Catalyst preparation

The CeO_2-WO_3 catalysts were prepared by using the co-precipitation method. Appropriate amounts of cerium nitrate and ammonium metatungstate were dissolved in an oxalic acid solution and mixed evenly. Excess urea solution was added with stirring, resulting in complete precipitation of a solid. The precipitated solids were collected by suction filtration, then washed with deionized water and dried overnight. Finally, after being calcined at 500 °C for 5h, the catalysts were crushed and sieved to 20−40 mesh before the activity tests. The samples are denoted as Ce_xW_y indicating the ratio of Ce to W atoms.

2.2 Catalyst characterization

Quantachrome QuadraSorb evo system was performed to measure N_2 adsorption-desorption isotherms of five CeO_2-WO_3 composite oxides samples at 77 K. The surface area (S_{BET}) was defined on the basis of Brunauer-

Emmett-Teller (BET) method to the adsorption isotherm in the relative pressure P/P_o of 0.00−0.32. The pore volume (V_{pore}) was calculated by the Barrett−Joyner−Halenda (BJH) method from the desorption isotherm.

The chemical composition and crystalline structure of samples were determined by X-ray diffraction (XRD, D/MAX2400, Rigaku Corporation) with Cu K_α radiation and in the range of 10°−90° (2 theta). X-ray photoelectron spectrometer (ESCALAB 250X, Thermo Fisher) was performed to record the X-ray photoelectron spectroscopy data of samples, using Al Kα X-ray source. The binding energies were calibrated using the C1s peak at 284.6 eV. For temperature programmed reduction (H_2-TPR) analysis, 50 mg catalyst was heated to 200 °C and purged with He for 1 h. After that, a mixture of 5% H_2/Ar (60 cm^3 min^{-1}) was purged into the reaction tube for TPR reaction. The temperature was increased at a rate of 10 °C min^{-1}, and the H_2 consumption was monitored by TCD detector. The thermogravimetric (TG) analysis of the materials which can be decomposed by heat was carried out by NETZSCH STA449F3 instrument. During the test process, N_2 was used as the carrier gas. The test temperature increased from room temperature to 900 °C, the rising rate was set as 10 °C min^{-1}. For Fourier transform infrared spectroscopy (FTIR) characterization of the catalysts, Nicolet5700 Fourier transform spectrometer was used in this work to characterize the sample.

2.3 Experimental setup

The schematic diagram of the experimental device is presented in Fig. 1. The typical inlet gas component was 500 ppm NO and 500 ppm NH_3, 3 vol% O_2, N_2 balance, 6 vol% H_2O (when used), 200 ppm SO_2 (when needed). In order to determine the influences of operating temperature on each process, the mixing units and SCR reactor were placed in the tubular furnace. The NH_3-SCR activities were measured in a fixed-bed quartz reactor with 16 mm inner diameter under atmospheric pressure from 100 °C to 450 °C. The total flow rate of the gas was maintained at 1.0 L min^{-1}, with the GHSV was approximately 25000 h^{-1}. The ozone generator structure used in the experiment was a coaxial cylindrical dielectric barrier discharge reactor. Power supply used in this experiment was a high frequency AC power supply (CTP-2000K). Mention that in this system the concentration of NO was excessive with respect to ozone, therefore ozone was consumed by the excessive NO before entering the catalyst system. A flue gas analyzer (Testo 350) was used to online monitor the concentration of NO and NO_2 in the simulated flue gas. Ozone was monitored by an ozone analyzer (2B Technologies). SO_2 and the composition of gas phase were determined by Fourier transform infrared spectroscopy (Nicolet 6700).

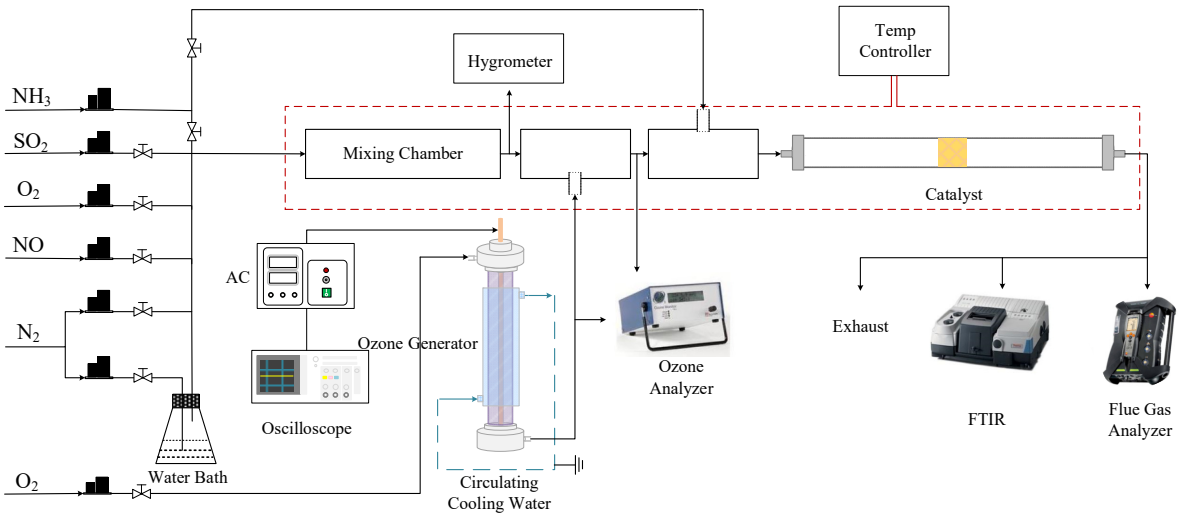

Fig. 1. Schematic of the experimental setup for O_3 assisted SCR system.

The NO oxidation rate and the NO_x removal efficiency were calculated according to the following equations:

$$NO_{conversion}(\%) = \frac{[NO]_{in} - [NO]_{out}}{[NO]_{in}} \times 100\% \quad (3)$$

$$NO_{x\,\text{removal}}\,(\%) = \frac{[NO_x]_{\text{in}} - [NO_x]_{\text{out}}}{[NO_x]_{\text{in}}} \times 100\% \quad (4)$$

where $[NO]_{in}$, $[NO_x]_{in}$ and $[NO]_{out}$, $[NO_x]_{out}$ represent the concentrations of NO and NO_x in the inlet and outlet gases respectively.

3. Results and discussion

3.1 Materials characterization

3.1.1 Structure characterization

In order to investigate the surface areas of mesoporous CeO_2-WO_3, we characterized the catalysts by using BET analysis. As shown in Table 1, it was found that the surface area of mesoporous CeO_2 was 18.93 $m^2\ g^{-1}$, which was smaller comparing to those of mesoporous Ce3W1 (28.22 $m^2\ g^{-1}$), Ce1W1 (22.02 $m^2\ g^{-1}$) and mesoporous Ce1W3 (22.74 $m^2\ g^{-1}$). The surface area apparently increased when CeO_2 was doped with WO_3. The order of the surface area was Ce3W1 > Ce1W3 > Ce1W1 > CeO_2, which was accordance with the catalytic activity. This result implies that the BET area is the main factor leading to the high activities of different mixed oxides [27].

Table 1. Physical parameters of the catalyst samples.

Samples	Specific area ($m^2\ g^{-1}$)	Pore diameter (nm)	Pore volume ($cm^3\ g^{-1}$)
CeO_2	18.93	0.48	0.14
Ce3W1	28.22	3.72	0.29
Ce1W1	22.02	3.94	0.15
Ce1W3	22.74	3.94	0.16
WO_3	7.20	1.76	0.08

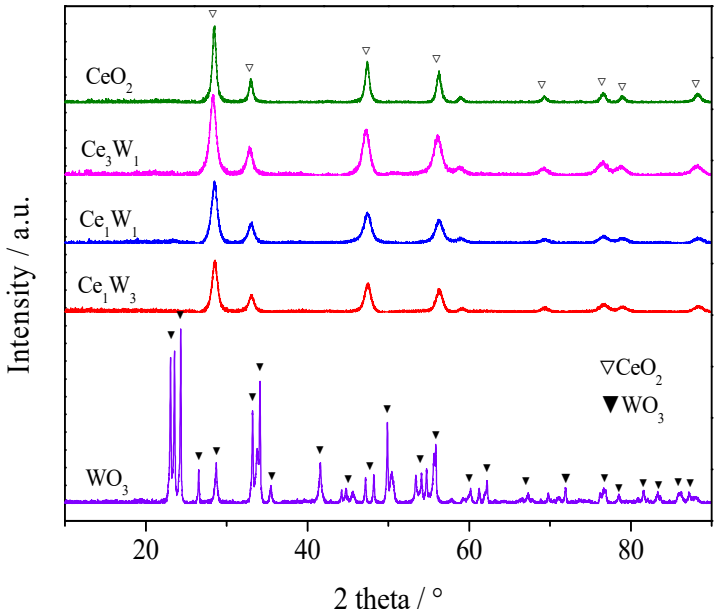

Fig. 2. XRD patterns of the CeO_2-WO_3 catalysts with different ratios of Ce/W.

The XRD patterns of the catalysts are shown in Fig. 2. The reflections of pure WO_3 and CeO_2 have provided typical diffraction patterns for the monoclinic WO_3 structure (PDF-ICDD 24-747) and the cubic CeO_2 structure (PDF-ICDD 34-394), and all peaks of different ratios of Ce/W catalysts can be designated as the cubic fluorite structure of CeO_2 [28]. With the results obtained through the XRD analysis, it can be concluded that the doping of WO_3 did not change the lattice structure of the CeO_2 catalyst. The diffraction peaks of WO_3 were not observed by XRD. This phenomenon can be caused by the reason that the entry of W^{6+} into the cubic fluorite structure of CeO_2 to form a solid solution since the ionic radii of Ce^{4+} and W^{6+} are respectively 0.92Å and 0.65Å, or another reason can be that WO_3 is highly dispersed on the surface of CeO_2 [29].

3.1.2 Redox properties

To obtain the information about the behavior of the catalyst in a reductive atmosphere and study the interaction between Ce and W species, H_2-TPR was performed. Fig. 3 shows the H_2-TPR profiles of the CeO_2-WO_3 catalysts with different ratios of Ce/W, pure CeO_2 and WO_3 in the temperature range of 200−900 °C. Three peaks were observed in the H_2-TPR spectrum of WO_3, with the maximum values at 604 °C, 703 °C, and 756 °C, respectively [30]. The H_2-TPR profile of CeO_2 at approximately 500 °C, 582 °C and 798 °C are associated with the stepwise reduction [31]. The onset consumption order was $CeO_2 < Ce_xW_y < WO_3$, indicating that due to the high thermal stability of WO_3, the reducible surface oxygen was suppressed or covered by WO_3. The H_2-TPR curves of the CeO_2-WO_3 catalyst with different ratios of Ce/W were similar to each other. The peak in the low temperature range of 500−600 °C was attributed to the reduction of CeO_2 to Ce_2O_3; another distinctly broad peak observed in the high temperature range of 750−800 °C represented the gradual reduction of W^{6+} to W^0 [32]. In addition, the doping of W caused the reduction peak of CeO_2-WO_3 catalyst to change to high temperature, which indicated that there was a synergy between Ce and W. Therefore, the difference in redox behavior between CeO_2-WO_3 catalyst and pure WO_3 and CeO_2 may be due to the interaction between Ce and W species.

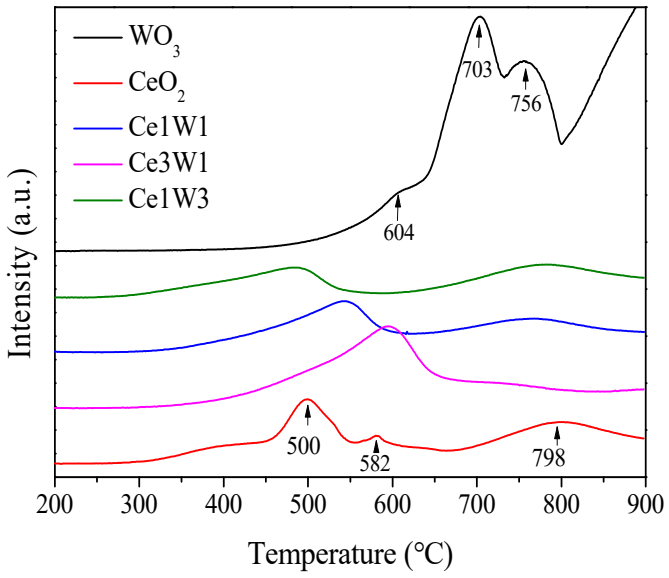

Fig. 3. H2-TPR patterns of the CeO_2-WO_3 catalysts with different ratios of Ce/W.

3.1.3 XPS analysis

XPS spectra were employed to further characterize the surfaces. The Ce3d, W 4f and O1s photoelectron profiles of Ce3W1, Ce1W1, Ce1W3, pure CeO_2 and WO_3 are shown in Fig. 4. The atomic concentrations and ratios are presented in Table 2.

Fig. 4 (a) shows the Ce3d spectra of Ce3W1, Ce1W1, Ce1W3 and pure CeO_2. The curve was divided into eight peaks by peak fitting [32]. From high binding energy to low binding energy, they were labeled v (916.7), v_1 (907.3), v_2 (903.7), v_3 (900.8), u (898.3), u_1 (888.6), u_2 (885.8), u_3 (882.7). Generally, regions with binding energy below 898.0 eV generally belong to Ce $3d_{5/2}$, while regions with binding energy above 900.4 eV belong to Ce $3d_{3/2}$; v_1 (907.3) and u_1 (888.6) correspond to Ce^{3+}, and the remaining peaks belong to the characteristic

peak of Ce^{4+} [32]. Therefore, Ce in different proportions of CeO_2-WO_3 catalyst existed in two valence states: Ce^{4+} and Ce^{3+}. Besides, WO_3 can play an important role in CeO_2-WO_3 catalyst, following the reaction (5) as below,

$$Ce^{4+}–NH_3 \rightarrow Ce^{3+} – NH_4^+ \quad (5)$$

the addition of W contributes to the transformation from Ce^{4+} to Ce^{3+} [33], which can result a higher $Ce^{3+}/(Ce^{3+}+Ce^{4+})$ ratio in CeO_2-WO_3 catalyst compared with pure CeO_2. Studies showed that Ce^{4+} and Ce^{3+} could form redox electron pairs on the surface of the catalyst, while a high proportion of Ce^{3+} can lead to lattice defects on the catalyst surface, which can accelerate the redox process between Ce^{4+} and Ce^{3+}, promote the storage and release of active oxygen, and finally increase the NO_x removal efficiency in the SCR process [34]. It can be seen from the figure 4 (a) that most of the Ce element in the CeO_2-WO_3 catalysts existed as Ce^{4+}. Therefore, the higher Ce^{3+} content in the catalyst indicated that imbalanced charges, vacancies, and unsaturated chemical bonds are formed on the catalyst surface, which was conducive to the adsorption and activation of NH_3 and NO [35]. According to Table 2, the $Ce^{3+}/(Ce^{3+}+Ce^{4+})$ ratios in the catalysts was in order of Ce3W1 > Ce1W1 > Ce1W3, which proved that the Ce3W1 catalyst can provide more oxygen vacancies.

Fig. 4 (b) shows the W 4f spectra of Ce3W1, Ce1W1, Ce1W3 and pure WO_3. Two peaks belong to W $4f_{7/2}$ and W $4f_{5/2}$ exist for all samples at 37.3−37.7 eV and 35.4−35.5 eV, respectively, which is correspond to the oxidation state W^{6+} of W. This is very close to the value reported by other researchers [36]. With the increase of the W doping amount, no significant change in the peak position was observed among these samples. This finding suggests that W^{6+} does not undergo a chemical change in these three catalysts, which is accordance with the XRD results.

The spectra of O1s for the five catalysts were investigated and the results are shown in Fig. 4 (c). The O1s peaks can be fitted into two peaks, the peak with high binding energy of 530.7−531.7eV were attributed to the surface chemisorbed oxygen (O_α) and the peak with low binding energy of 528.5−530.5 eV were assigned to the surface lattice oxygen (O_β). As is well-known, O_α is highly active in oxidation reactions due to its higher mobility than the lattice oxygen O_β [37]. From Table 2 it can be obtained that identifying with the trend of the $Ce^{3+}/(Ce^{3+}+Ce^{4+})$ ratio, the O_α ratio in Ce3W1 was the highest, followed by the Ce1W1 and Ce1W3. It also indicates that when WO_3 was added to the pure CeO_2 catalyst, the O_α ratio of the CeO_2-WO_3 catalyst increased significantly, which can be ascribed to the increase of $Ce^{3+}/(Ce^{3+}+Ce^{4+})$ ratio. It has been reported that once Ce^{3+} presents in the CeO_2, oxygen vacancies will be generated to maintain electrostatic balance according to the following process [38]:

$$4Ce^{4+} + O^{2-} \rightarrow 4Ce^{4+} + 2e^-/\square + 0.5O_2 \rightarrow 2Ce^{4+} + 2Ce^{3+} + \square + 0.5O_2 \quad (6)$$

Where □ represents an empty position, which originates from the removal of O^{2-} from the lattice. In this situation, the generation of additional chemisorbed oxygen or weakly adsorbed oxygen species could occur on the surface of the catalyst. In addition, W^{n+} could form vacancies and unsaturated bonds such as W = O on the catalyst surface, which leads to oxide defects and the increase of hydroxyl-like groups. Subsequently, the increase of hydroxyl group on the catalyst surface was conducive to the adsorption of ammonia gas and the formation of NH^{4+} and therefore, more Brönsted acid sites can be formed [39].

Table 2. XPS results for various catalysts.

Sample	$Ce^{3+}/(Ce^{3+}+Ce^{4+})$ (%)	O_α/O_{total} (%)
Ce	13.5	21.9
Ce3W1	19.2	62.4
Ce1W1	16.5	32.7
Ce1W3	16.0	24.6
W	–	92.7

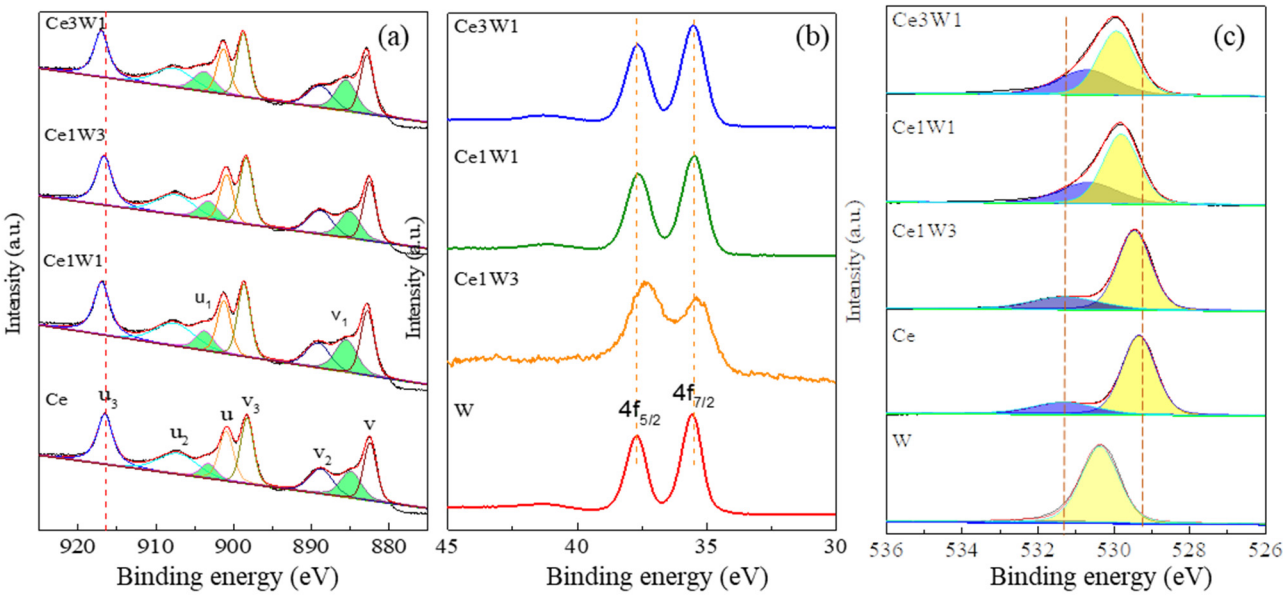

Fig. 4. XPS spectra of the CeO_2-WO_3 catalysts with different ratios of Ce/W: (a) Ce3d; (b) W4f; (c) O1s.

3.2 SCR catalytic activity

Fig.5 shows the SCR activity of pure CeO_2, pure WO_3 and CeO_2-WO_3 mixed oxides catalysts in the temperature range of 100−450 °C under a GHSV of 25 000 h^{-1}. For pure CeO_2 catalyst, the NO_x conversion rate is low in the low temperature and shows a high NO_x conversion of 71.8% in the temperature of 350 °C. For pure WO_3 catalyst, there is almost no denitration efficiency below 200 °C. However, the SCR denitration efficiency reached 83.1% at 450 °C, and the catalytic activity of the catalyst gradually increased with the increase of temperature over 200 °C. It can be indicated that WO_3 presents a higher activity than CeO_2 at high temperature, which indicates WO_3 possesses a better resistance to high temperatures. When WO_3 is doped in the pure CeO_2 catalyst, the activity of the catalyst is significantly improved. Compared with pure CeO_2, the activation temperature window of CeO_2-WO_3 catalysts with different Ce/W molar ratios was widened. The NO_x removal rate of Ce1W1 gradually increased with the increase of temperature, and the best effect was 88.6% when the temperature reached 400°C. The activity of Ce1W3 catalyst increases rapidly at 200 °C, and NO_x is close to 100% in the temperature range of 250−350 °C. Among these, the Ce3W1 catalyst supplied the best catalytic activity and the widest active temperature window. Compared with other catalysts, the NO_x conversion for Ce3W1 shows the highest conversion performance before 200 °C and can reach nearly 100% at 250−400 °C. It has been reported that as a stabilizer and accelerator, W can significantly increase the specific surface area of the catalyst [40]. The highly dispersed W element is conducive to the improvement of the catalytic effect of the catalyst and broaden the reaction temperature window of the catalyst [41]. However, the load of W could also affect the catalyst activity as illustrated in the BET and XPS analysis and subsequently influences the catalytic performance. Herein as the same result from foregoing analysts, the highest catalytic performance of NO_x conversion and the largest surface area and Oα ratio were simultaneously obtained when the ration of Ce/W reaches 3:1. Therefore, due to the superiority of Ce3W1 catalyst in the NO reduction, it is used in all the following experiments.

3.3 Ozone assisted SCR catalytic activity

The operating temperature is a critical parameter for ozone assisted SCR. At higher temperatures, O_3 can be decomposed to O_2 and O, which leads to a reduction in the conversion rate of NO [42]. The denitration efficiency of the O_3-SCR process at low temperatures (< 200 °C) is shown in Figure 6. It can be seen that the denitration effect of O_3-SCR process was significantly higher than that of standard SCR. For example, the denitration efficiency of SCR at 150 °C is only 63.9%, while the O_3-SCR flue gas denitration efficiency reaches 90.3%, which exists an increase of 26.4%. The results suggest that the SCR process of O_3-SCR could significantly improve NO_x removal efficiency in a lower temperature window.

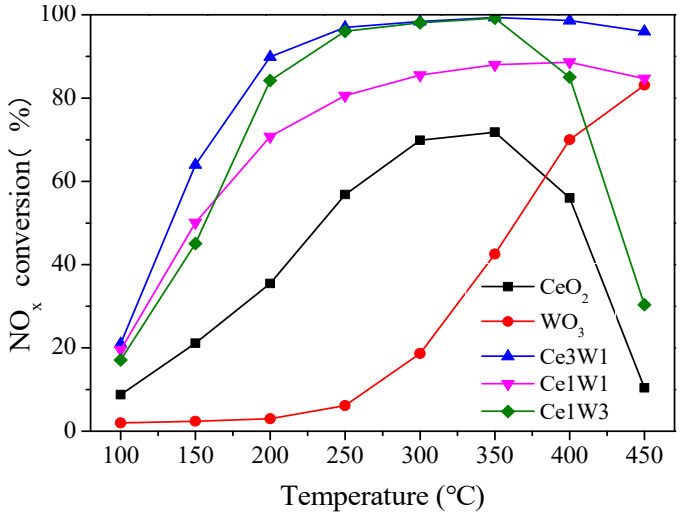

Fig. 5. NO_x conversion over pure CeO_2, pure WO_3 and CeO_2-WO_3 mixed oxides catalysts.

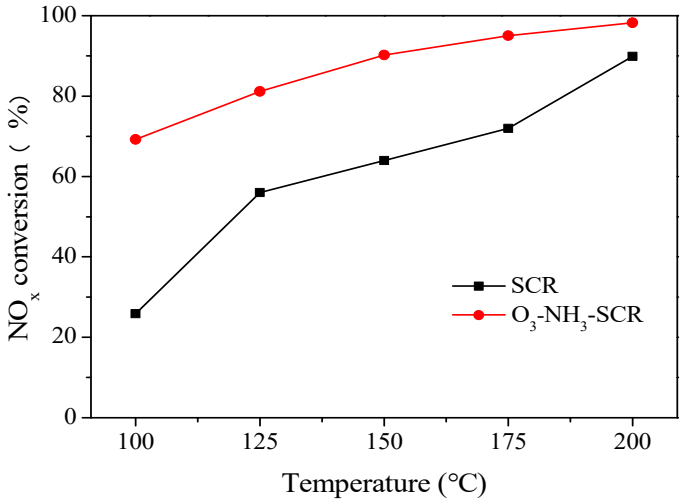

Fig. 6. NO_x conversion of ozone assisted SCR process.

3.4 Effect of SO_2 on NO_x removal efficiency

3.4.1 Comparison of SO_2 poisoning effects on NO_x conversion between O_3-SCR and SCR processes

As mentioned above, SO_2 poisoning is currently a major problem in the field of low temperature denitration. Therefore, this paper investigated whether the catalysts have different performances and mechanisms against SO_2 poisoning in the O_3-SCR process and the standard SCR process. Fig.7 shows the influence of SO_2 on NO_x conversion for Ce3W1 at 150 °C. When SO_2 did not exist in the system, NO conversion efficiency of SCR and O_3-SCR could be maintained at about 63% and 90%, respectively. After 200 ppm SO_2 was introduced, the NO conversion of SCR and O_3-SCR dropped to 40% and 69% within 5 hours, and then gradually decreased over time. The result shows that with the introduction of SO_2, the change of NO removal efficiency is controlled by different reaction mechanisms. The catalysts in O_3-SCR and SCR were poisoned by SO_2, but the efficiency of O_3-SCR denitration was still significantly better than that of SCR. It has been found that the gradual decrease in NO conversion in SCR was due to the deposition of ammonium sulfate [43]. However, few studies have focused on the effects of O_3-SCR on catalysts' resistance to SO_2 poisoning. Therefore, the subsequent studies used various catalyst characterization methods to explore the mechanism of catalyst resistance to SO_2 poisoning in two processes.

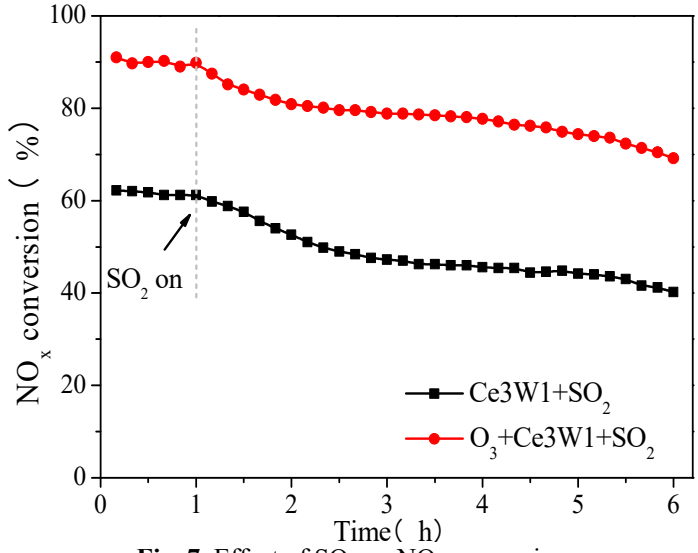

Fig. 7. Effect of SO_2 on NO_x conversion.

3.4.2 XRD and FTIR results

In order to identify the change of crystalline phases for the fresh and sulfur poisoned Ce3W1 catalyst. XRD measurements were carried out and the patterns are shown in Fig. 8. For the fresh Ce3W1 catalyst, sharp diffraction peaks are obtained. After poisoned with SO_2, the intensity of each peak decreases, especially for the catalyst after SO_2 treatment in SCR, indicating the obvious crystal structure damage of Ce3W1 after adding SO_2 for 5 h at 150 °C..

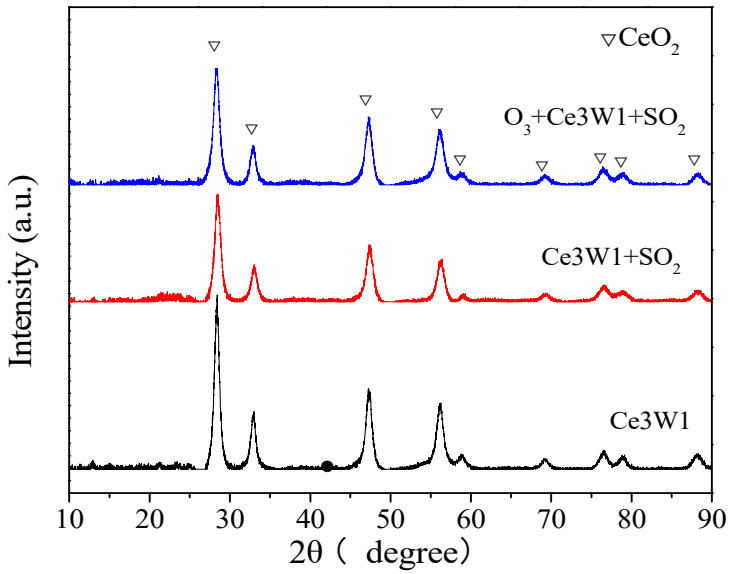

Fig. 8. The XRD pattern of catalysts before and after SO_2 atmosphere reaction.

To investigate the SO_2-poisoned mechanism further, IR analysis of product species in SO_2 poisoned catalysts were performed. Fig.9 shows the results of IR analysis of the sample after 5 h reaction in sulfur-containing flue gas. The weak peaks observed in Ce3W1 catalyst at 1132 cm^{-1} and 1043 cm^{-1} are corresponding to the characteristic band of sulfate ion [44]. Meanwhile, it was reported that the massive sulfate produced by the oxidation of SO_2 on cerium is characterized by a very wide band around 1000–1200 cm^{-1} [45]. The peak at 1385 cm^{-1} was attributed to the monodentate nitrite species, as intermediate product generated from the SCR [46]. The absorption bands at 3420 cm^{-1} and 1640 cm^{-1} corresponded to the O−H stretching vibration peak of the adsorbed water and the bending vibration band of the surface O−H groups, respectively. In particular, the N−H vibration band of coordinated NH_3 and ionic NH^{4+} in the range of 3000–4000 cm^{-1} may overlap with the O−H stretching vibration band [47].

Additionally, sulfite was not detected by IR characterization. Based on these results, it was deduced that SO_2 was firstly adsorbed on the catalyst and then reacted with the support or active ingredient. Eventually, sulfate deposits were generated in the active center, which blocked the active channel of the catalyst and resulted in catalyst deactivation.

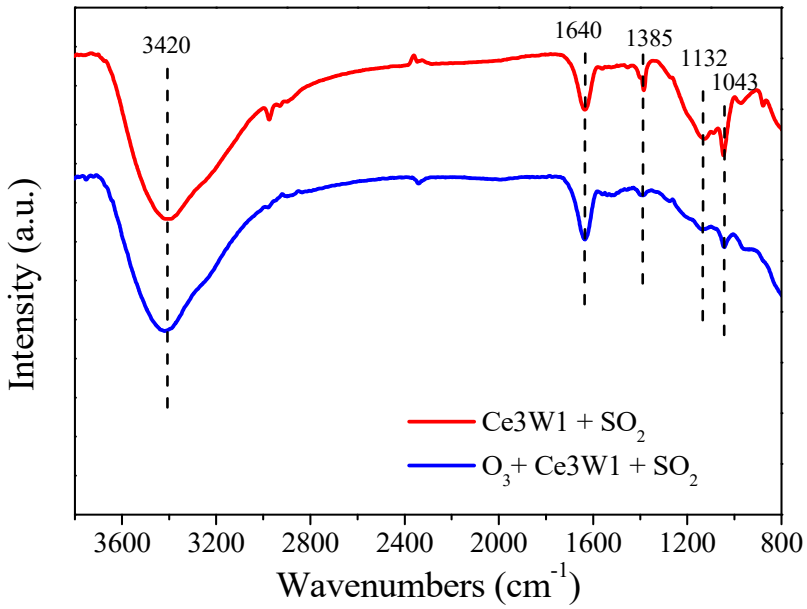

Fig. 9. The FTIR spectrograms of catalysts after SO_2 atmosphere reaction.

3.4.3 XPS analysis

The XPS technique was performed to explore the transformation of the surface chemical composition of the Ce3W1 catalyst in the presence of SO_2. Results of XPS analysis for the samples are reported in Fig. 10. The resultant surface elemental concentration and surface atomic ratio are summarized in Table 3. Figs. 10 (a) and 10 (b) show that the binding energy of Ce3d and O1s in the catalyst after SO_2 poisoning was basically the same as that in Fig. 4 (a). The valence composition of Ce and O elements did not change. Ce^{3+} (v1 and u1) and Ce^{4+} (v, v2, v3, u, u2, and u3) were the valence states of the Ce element, and surface chemisorbed oxygen (O_α) and lattice oxygen (O_β) were also the valence states of the O element. For the SCR and ozone assisted SCR processes, after 5 hours under 200 ppm SO_2 conditions, the Ce3W1 catalyst had a slight increase in $Ce^{3+}/(Ce^{3+} + Ce^{4+})$ ratio from 19.2% to 25.7%, 25.2%, respectively. However, the proportion of O_α in SO_2 poisoned catalyst decreased significantly from 62.4% to 38.8% and 30.4%, respectively.

Meanwhile, the XPS spectrum of S2p detected on the catalyst surface after reaction is shown in Fig. 10 (c). It can be obtained that sulfur element existed in the form of sulfate and sulfite. The peak at 168.1 eV was designated as the formation of surface SO_3^{2-} species, while the higher binding energies included 168.6 eV and 169.5 eV was assigned to the formation of surface SO_4^{2-} species [45]. The increase of Ce^{3+} content and the presence of SO_4^{2-} species on the surface indicated that $Ce_2(SO_4)_3$ was produced after the reaction of SO_2 and Ce3W1 [48]. It is worth noting that Fig. 10 (c) and Table 3 clearly show that the sulfur content of Ce3W1 in SCR was significantly higher than that of the O_3-SCR, which means that the addition of ozone could reduce the formation of sulfate species.

Table 3. XPS results for various catalysts.

Samples	Surface composition/mol.%			$Ce^{3+}/(Ce^{3+}+Ce^{4+})$ (%)	O_α/O_{total} (%)
	Ce	O	S		
Ce3W1	–	–	–	19.2	62.4
Ce3W1+SO_2	20.02	75.42	4.56	25.7	38.8
O_3+Ce3W1+SO_2	21.34	75.87	2.79	25.2	30.4

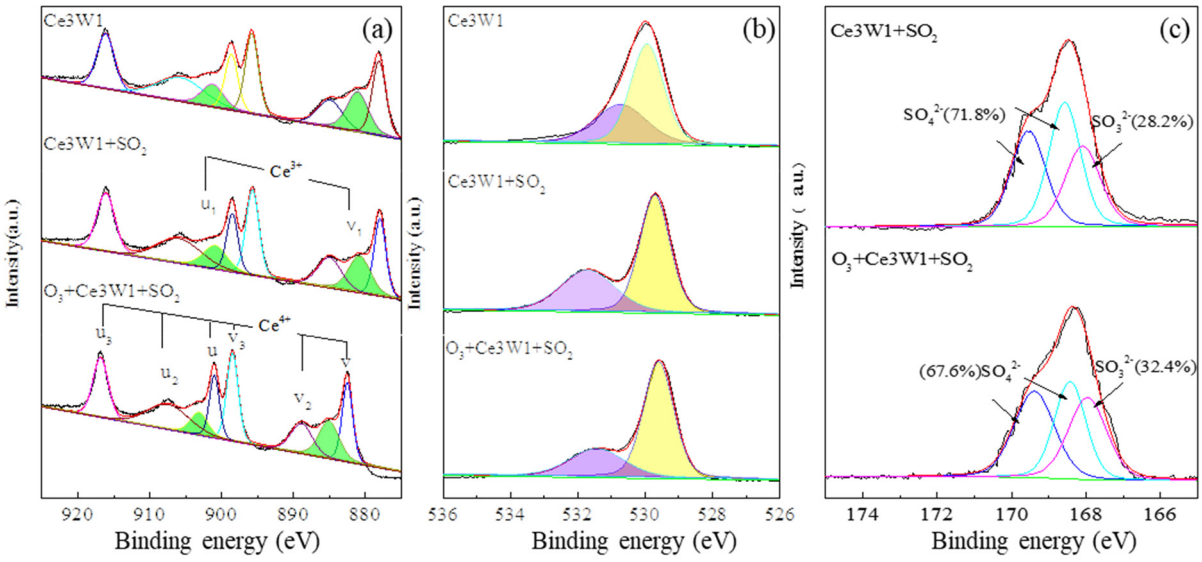

Fig. 10. XPS spectra of (a) Ce3d, (b) O1s, and (c) S2p for the samples.

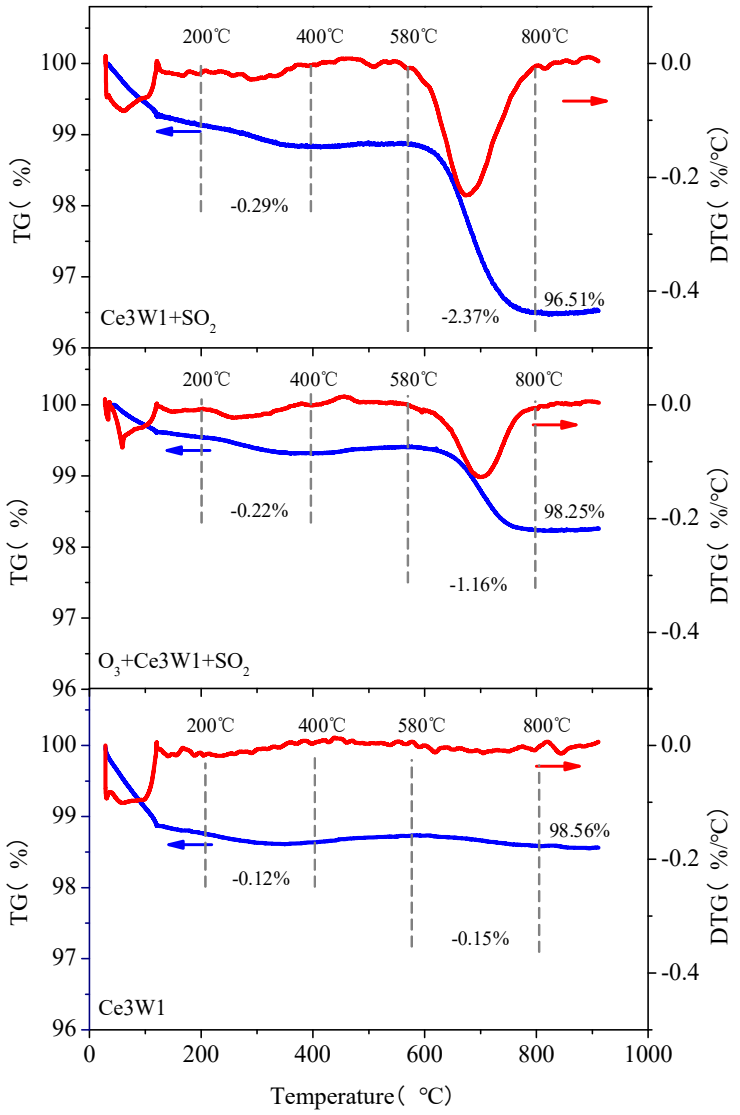

Fig. 11. TG-DTG curves of catalysts after different processes.

3.4.4 TG results

Fig. 11 shows the weight loss of the catalysts before and after the SO_2 test in the TG. The catalysts included the fresh Ce3W1, SO_2 poisoned Ce3W1 (5 h) in SCR and SO_2 poisoned Ce3W1 (5 h) in O_3-SCR, here the Ce3W1 (5 h) refers to a spent catalyst tested in a SO_2-contaning flue gas for 5 hours with the temperature of 150 °C. The TG curve presented three major weigh losses and the DTG curve displayed three corresponding valleys for SO_2 poisoned catalyst. The first stage is between 30 °C and 100 °C, which is mainly caused by the evaporation of water adsorbed on the catalyst surface [49]. The second stage between 200 °C and 400 °C could be owed to the thermal decomposition of NH_4HSO_4 and $(NH_4)_2SO_4$, which was similar to the thermal decomposition temperatures of $(NH_4)_2SO_4$ and NH_4HSO_4 reported in the literature at 230 °C and 350 °C, respectively [45]. The third stage between 580 °C and 800 °C could be attributed to the decomposition of cerium sulfate [50]. The fresh Ce3W1 catalyst only showed significant weight loss before 100 °C, and the weight loss was relatively gentle in the temperature range of 200–400 °C and 580–800 °C. However, the peak mass loss of the ammonium sulfate (hydrogen) ammonium salt on the catalyst in the SCR and the catalyst of the O_3-SCR was respectively 0.29% and 0.22%. Meanwhile, for the weight loss peak of cerium sulfate, the mass loss was 2.37% and 1.16%, respectively. From the above TG results, it could be seen that when SO_2 was contained in the flue gas, the Ce3W1 catalyst inevitably produced ammonium sulfate (hydrogen) sulfate and cerium sulfate. Apparently, O_3-SCR produced less sulfate than SCR. The TG/DTG results further proved that the O_3-SCR process could reduce the toxic effect of SO_2 on the catalyst and extend the service life of the catalyst.

4. Conclusion

CeO_2-WO_3 catalysts with different proportion of Ce/W were prepared by co-precipitation method and Ce3W1 was screened for the optimization of the high NH_3-SCR activity in a wide temperature range. The NO_x conversion performance of the O_3-SCR was investigated, and it was found that the O_3-SCR could significantly improve the NO_x removal efficiency at low temperature. SO_2 resistance performance of CeO_2-WO_3 catalysts was compared in O_3-SCR and standard SCR two systems. In a simulated flue gas containing 200 ppm SO_2, the catalytic activity of the O_3-SCR and SCR process catalyst decreased obviously at 150 °C after 5 h of continuous test. XPS, FTIR and TG analysis of SO_2 poisoned catalysts depicted that a small amount of sulfate species (NH_4HSO_4, $(NH_4)_2SO_4$, $Ce_2(SO_4)_3$) were formed and deposited on the surface of the O_3-SCR compared with the standard SCR. It was further clarified that O_3-SCR could obviously improve NO_x removal at lower temperatures, and could also reduce the poisoning effect of SO_2 on the catalyst. Therefore, the technology of O_3-SCR has broad prospects for practical application.

Acknowledgment

This work has been supported by National Natural Science Foundation of China (Grant No. 51877027 and No. 51877028).

References

[1] Wei C.C., Lin H.J., Lim Y.P., Chen C.S., Chang C.Y., Lin C.J., Chen J.Y., Tien P.T., Lin C.L., and Wan L., PM 2.5 and NO_x exposure promote myopia: clinical evidence and experimental proof, *Environ. Pollut*., Vol. 254, pp. 113031, 2019.

[2] Sun W.Q., Zhou Y., Lv J.X., and Wu J.Z., Assessment of multi-air emissions: Case of particulate matter (dust), SO_2, NO_x and CO_2 from iron and steel industry of China, *J. Cleaner Prod.*, Vol. 232, pp. 350−358, 2019.

[3] Colombo M., Nova I., and Tronconi E., Detailed kinetic modeling of the NH_3–NO/NO_2 SCR reactions over a commercial Cu-zeolite catalyst for Diesel exhausts after treatment, *Catal. Today*., Vol. 197, pp. 243−255, 2012.

[4] Tronconi E., Nova I., and Ciardelli C., Redox features in the catalytic mechanism of the "standard" and "fast" NH_3-SCR of NO_x over a V-based catalyst investigated by dynamic methods, *J. Catal*., Vol. 245, pp. 1−10, 2007.

[5] Iwasaki M., and Shinjoh H., A comparative study of "standard", "fast" and "NO_2" SCR reactions over Fe/zeolite catalyst, *Appl. Catal., A*., Vol. 390, pp. 71−77, 2010.

[6] Liu M.Y, Li J., Liu Z.Y., Jiang N., Wu Y., Improve low-temperature selective catalytic reduction of NO_x with NH_3 by ozone injection. *Int. J. Plasma Environ. Sci. Technol*., Vol. 14 (1), e01007 (11pp), 2020.
[7] Shao J., Xu C., Wang Z., Zhang Z.P., Wang R.T., He Y., and Cen K.F., NO_x reduction in a 130 t/h biomass-fired circulating fluid bed boiler using coupled ozonation and wet absorption technology, *Ind. Eng. Chem. Res*., Vol. 58 (39), pp. 18134−18140, 2019.
[8] Chen H.L., Lee H.M., Chen S.H., and Chang M.B., Review of packed-bed plasma reactor for ozone generation and air pollution control, *Ind. Eng. Chem. Res*., Vol. 47 (7), pp. 2122−2130, 2008.
[9] Chen M., Takashima K., and Mizuno A., Plasma assisted NO_x removal using modified attapulgite clay catalyst, *Int. J. Plasma Environ. Sci. Technol.*, Vol. 6 (1), pp. 81−84, 2012.
[10] Kulstra W.S., Biervliet M., Poels E.K., and Bliek A., Deactivation by SO_2 of MnO_x/ Al_2O_3 catalysts used for the selective catalytic reduction of NO with NH_3 at low temperatures, *Appl. Catal., B*., Vol. 16, pp. 1327−337,1998.
[11] Kim H.H., Ayman A.A., Teramoto Y., Nozaki T., Hensel K., Mok Y.S., Shirjana S., Duc B.N., Lee D.H., and Kang W.S., Interim report of plasma catalysis: Footprints in the past and blueprints for the future, *Int. J. Plasma Environ. Sci. Technol.*, Vol. 15 (1), e01004 (39pp), 2021.
[12] Liu F. and He H., Selective catalytic reduction of NO with NH_3 over manganese substituted iron titanate catalyst: Reaction mechanism and H_2O/SO_2 inhibition mechanism study, *Catal. Today*., Vol. 153, pp. 70−76, 2010.
[13] Liu Y.M., Shu H., Xu Q.S., Zhang Y.H., and Yang L.J., FT-IR study of the SO_2 oxidation behavior in the selective catalytic reduction of NO with NH_3 over commercial catalysts, *J Fuel Chem Technol*., Vol. 43, pp. 1018−1024, 2015.
[14] Jiang X., Xu W., Lai S., and Chen X., Integral structured Co-Mn composite oxides grown on interconnected Ni foam for catalytic toluene oxidation, *RSC Adv*., Vol. 9, pp. 6533−6541, 2019.
[15] Luis J.A., Luca L., Natale F., Pio F., Guido B., Elio G., and Fiorenzo B., Reactivity and physicochemical characterization of V_2O_5-WO_3/TiO_2 De-NO_x catalysts, *J. Catal*., Vol. 155, pp. 117−130, 1995.
[16] Yu J., Guo F., Wang Y.L., Zhu J.H., Liu Y.Y., Su F.B., Gao S.Q., and Xu G.W., Sulfur poisoning resistant mesoporous Mn-base catalyst for low-temperature SCR of NO with NH_3, *Appl. Catal., B*, Vol. 95, pp. 160−168, 2010.
[17] Kapteijn F., Singoredjo L., Andreini A., and Moulijn, J., Activity and selectivity of pure manganese oxides in the selective catalytic reduction of nitric oxide with ammonia, *Appl. Catal., B*., Vol. 3, pp. 173−189, 1994.
[18] Yan Z.D., Shan W.P., Shi X.Y., He G.Z., Lian Z.H., Yu Y.B., Shan Y.L., Liu J.J., and He H., The way to enhance the thermal stability of V_2O_5-based catalysts for NH_3-SCR, *Catal. Today*, Vol. 355, pp. 408−414, 2020.
[19] Wu X., Meng H., Du Y.L., Liu J.N., Hou B.H. and Xie X.M., Insight into Cu_2O/CuO collaboration in the selective catalytic reduction of NO with NH_3: Enhanced activity and synergistic mechanism, *J. Catal*., Vol. 384, pp. 72−87, 2020.
[20] Wang H.M., Ning P., Zhang Y.Q., Ma Y.P., Wang J.F., Wang L.Y. and Zhang Q.L., Highly efficient WO_3-FeO_x catalysts synthesized using a novel solvent-free method for NH_3-SCR, *J. Hazard. Mater.*, Vol. 388, 121812, 2019.
[21] Xu W.Q., Yu Y.B., Zhang C.B. and He H., Selective catalytic reduction of NO by NH_3 over a Ce/TiO_2 catalyst, *Catal. Commun.*, Vol. 9, pp. 1453−1457, 2008.
[22] Guo R.T., Zhen W.L., Pan W.G., Zhou Y., Jie-Nan H., Xu H.J., Jin Q., Ding C.G., and Guo S.Y., Effect of Cu doping on the SCR activity of CeO_2 catalyst prepared by citric acid method, *J. Ind. Eng. Chem*., Vol. 20 (4), pp. 1577−1580, 2014.
[23] Wang Z.H., Lin F.W., Jiang S.D., Qiu K.Z., Kuang M., Whiddon R., and Cen K.F., Ceria substrate–oxide composites as catalyst for highly efficient catalytic oxidation of NO by O_2, *Fuel*, Vol. 166, pp. 352−360, 2016.
[24] Michael D.A., Robert V.D., and Israel E.W., The effect of metal oxide additives on the activity of V_2O_5/TiO_2 catalysts for the selective catalytic reduction of nitric oxide by ammonia, *Appl. Catal., B*., Vol. 20, pp. 111−122, 1999.
[25] Kobayashi M., and Miyoshi K., WO_3–TiO_2 monolithic catalysts for high temperature SCR of NO by NH_3: Influence of preparation method on structural and physico-chemical properties, activity and durability, *Appl. Catal., B*., Vol. 72, pp. 253−261, 2007.
[26] Zhang Y.P., Wang X.L., Shen K., Xu H.T., Sun K.Q., and Zhou C.C., WO_3 modification of MnO_x/TiO_2 catalysts for low temperature selective catalytic reduction of NO with ammonia, *Chin. J. Catal*., Vol. 33, pp. 1523−1531, 2012.
[27] Chang H.Z., Li J.H., Chen X.Y., Ma L., Yang S.J., Schwank J.W., and Hao J.M., Effect of Sn on MnO_x-CeO_2 catalyst for SCR of NO_x by ammonia: Enhancement of activity and remarkable resistance to SO_2, *Catal. Commun.*, Vol. 27, pp. 54−57, 2012.
[28] Peng, Y., Wang C.Z., and Li J.H., Structure-activity relationship of VO_x/CeO_2 nanorod for NO removal with ammonia, *Appl. Catal., B*., Vol. 144, pp. 538−546, 2014.
[29] Chen L., Li J.H., Ge M.F., Lei M., and Cheng H.Z., Mechanism of selective catalytic reduction of NO_x with NH_3 over CeO_2-WO_3 catalysts, *Chin. J. Catal.*, Vol. 32, pp. 836−841, 2011.
[30] Ma Z.R., Weng D., Wu X.D., and Si Z.C., Effects of WO_x modification on the activity, adsorption, and redox properties of CeO_2 catalyst for NO_x reduction with ammonia, *J. Environ. Sci*., Vol. 24 (7), pp. 1305−1316, 2012.
[31] Xiong Y., Tang C.J., Yao X.J., Zhang L., Li L.L., Wang X.B., Deng Y., Gao F., and Dong, L., Effect of metal ions doping (M=Ti^{4+}, Sn^{4+}) on the catalytic performance of MnO_x/CeO_2 catalyst for low temperature selective catalytic reduction of NO with NH_3, *Appl. Catal., A*., Vol. 495, pp. 206−216, 2015.

[32] Gao X., Jiang Y., Fu Y.C., Zhong Y., Luo Z.Y. and Cen K.F., Preparation and characterization of CeO_2/TiO_2 catalysts for selective catalytic reduction of NO with NH_3, *Catal. Commun*., Vol. 11, pp. 465−469, 2010.
[33] Chen L.A., Li J.H., and Ge M.F. DRIFT Study on Cerium-Tungsten/Titiania Catalyst for Selective Catalytic Reduction of NO_x with NH_3, *Environ. Sci. Technol.*, Vol.44, pp.9590–9596, 2010.
[34] Wang X.Q., Liu Y., and Wu Z.B., Highly active $NbOPO_4$ supported Cu-Ce catalyst for NH_3-SCR reaction with superior sulfur resistance, *Chem. Eng. J.*, Vol. 382, 122941, 2020.
[35] Fang C., Zhang D.S., Shi L.Y., Gao R.H., Li H.R., Ye L.P., and Zhang J.P., Highly dispersed CeO_2 on carbon nanotubes for selective catalytic reduction of NO with NH_3, *Catal. Sci. Technol*., Vol. 3, pp. 803−811, 2013.
[36] He Y.Y., Ford M.E., Zhu M.H., Liu Q.C., Tumuluri U., Wu Z.L., and Wachs I.E., Influence of catalyst synthesis method on selective catalytic reduction (SCR) of NO by NH_3 with V_2O_5-WO_3/TiO_2 catalysts, *Appl. Catal., B*., Vol. 193, pp. 141−150, 2016.
[37] Zhang L., Zou W.X., Ma K.L., Cao Y., Xiong Y., Wu S.G., Tang C.J., Gao F., and Dong L., Sulfated temperature effects on the catalytic activity of CeO_2 in NH_3-selective catalytic reduction conditions, *J. Phys. Chem. C*., Vol. 119, pp. 1155−1163, 2014.
[38] Liu X.W., Zhou K.B., Wang L., Wang B.Y., and Li Y.D., Oxygen vacancy clusters promoting reducibility and activity of ceria nanorods, *J. Am. Chem. Soc.*, Vol. 131 (9), pp. 3140–3141,2009.
[39] Liu C.X., Chen L., Chang H.Z., Ma L., Peng Y., Arandiyan H., and Li J.H., Characterization of CeO_2-WO_3 catalysts prepared by different methods for selective catalytic reduction of NO_x with NH_3, *Catal. Commun*., Vol. 40, pp. 145−148, 2013.
[40] Chen L.A., Li J.H., Ablikim W., Wang J., Chang H.Z., Ma L., Xu J.Y., Ge M.F., and Arandiyan H., CeO_2–WO_3 mixed oxides for the selective catalytic reduction of no_x by nh_3 over a wide temperature range, *Catal Lett.*, Vol. 141, pp. 1859–1864, 2011.
[41] Motonobu K., and Katsunori M., WO_3–TiO_2 monolithic catalysts for high temperature SCR of NO by NH_3: Influence of preparation method on structural and physico-chemical properties, activity and durability, *Appl. Catal., B.*, Vol. 72, pp. 253–261, 2007.
[42] Wang Z., Cen K., and Zhou J., Simultaneous multi-pollutants removal in flue gas by ozone, Springer, 2014.
[43] Sheng Z.Y., Hu Y.F., Xue J.M., Wang X.M., and Liao W.P., SO_2 poisoning and regeneration of Mn-Ce/TiO_2 catalyst for low temperature NO_x reduction with NH_3, *J. Rare Earths*., Vol. 30, pp. 676−682, 2012.
[44] Wang F.M., Shen B.X., Zhu S.W., and Wang Z., Promotion of Fe and Co doped Mn-Ce/TiO_2 catalysts for low temperature NH_3-SCR with SO_2 tolerance, *Fuel*., Vol. 249, pp. 54−60, 2019.
[45] Wu Z.B., Jin R.B., Wang H.Q., and Liu Y., Effect of ceria doping on SO_2 resistance of Mn/TiO_2 for selective catalytic reduction of NO with NH_3 at low temperature, *Catal. Commun*., Vol. 10, pp. 935-939, 2009.
[46] Ma Z.X., Yang H.S., Li Q., Zheng J.W., and Zhang X.B., Catalytic reduction of NO by NH_3 over Fe–Cu–O_X/CNTs-TiO_2 composites at low temperature, *Appl. Catal., A*., Vol. 427–428, pp. 43−48, 2012.
[47] Zhang A.C., Zhang Z.H., Lu H., Liu Z.C., Jun X., Zhou C.S., Xing W.B., and Sun L.S., Effect of promotion with Ru addition on the activity and SO_2 resistance of MnO_x−TiO_2 adsorbent for HgO removal, *Ind. Eng. Chem. Res*., Vol. 54 (11), pp. 2930−2939, 2015.
[48] Gao F.Y., Tang X.L., Yi H.H., Li J.Y., Zhao S.Z., Wang J.G., Chu C., and Li C.L., Promotional mechanisms of activity and SO_2 tolerance of Co- or Ni-doped MnO_x-CeO_2 catalysts for SCR of NO_x with NH_3 at low temperature, *Chem. Eng. J*., Vol. 317, pp. 20−31, 2017.
[49] Zhang L., Li L.L., Cao Y., Yao X.J., Ge C.Y., Gao F., Deng Y., Tang C.J., and Dong L., Getting insight into the influence of SO_2 on TiO_2/CeO_2 for the selective catalytic reduction of NO by NH_3, *Appl. Catal., B*., Vol. 165, pp. 589−598, 2015.
[50] Zhang L., Zou W.X., Ma K.L., Cao Y., Xiong Y., Wu S.G., Tang C.J., Gao F., and Dong L., Sulfated temperature effects on the catalytic activity of CeO_2 in NH_3-selective catalytic reduction conditions, *J. Phys. Chem. C*., Vol. 119 (2), pp. 1155−1163, 2015.